Observation of Half-Quantum Vortices in Topological Superfluid ^{3}He

S. Autti,[1,*] V. V. Dmitriev,[2] J. T. Mäkinen,[1] A. A. Soldatov,[2,3] G. E. Volovik,[1,4] A. N. Yudin,[2] V. V. Zavjalov,[1] and V. B. Eltsov[1]

[1]*Low Temperature Laboratory, Department of Applied Physics, Aalto University, P.O. Box 15100, FI-00076 AALTO, Finland*
[2]*P. L. Kapitza Institute for Physical Problems of RAS, 119334 Moscow, Russia*
[3]*Moscow Institute of Physics and Technology, 141700 Dolgoprudny, Russia*
[4]*Landau Institute for Theoretical Physics, 142432 Chernogolovka, Russia*

(Received 24 August 2016; published 14 December 2016)

One of the most sought-after objects in topological quantum-matter systems is a vortex carrying half a quantum of circulation. They were originally predicted to exist in superfluid ^{3}He-*A* but have never been resolved there. Here we report an observation of half-quantum vortices (HQVs) in the polar phase of superfluid ^{3}He. The vortices are created with rotation or by the Kibble-Zurek mechanism and identified based on their nuclear magnetic resonance signature. This discovery provides a pathway for studies of unpaired Majorana modes bound to the HQV cores in the polar-distorted *A* phase.

DOI: 10.1103/PhysRevLett.117.255301

Topology reveals unified features in quantum-matter systems as diverse as the chiral *A* phase of superfluid ^{3}He at temperatures $T \sim 10^{-3}$ K and the vacuum of the standard model at $T \sim 10^{15}$ K [1]. Those common topological properties are manifested in supported topological defects (like vortices, Skyrmions, etc.) and gapless quasiparticle states. Superfluid phases of ^{3}He provide a versatile platform for studying topological properties of quantum matter [1,2]. One of the most striking consequences of nontrivial topology is a vortex which carries half a quantum of circulation in a superfluid or of magnetic flux in a superconductor. Such vortices are also predicted to host core-bound unpaired Majorana modes [3–5]. The search for half-quantum vortices (HQVs) began in chiral Weyl superfluid ^{3}He-*A* in the late 1970s. Despite promising theoretical predictions, HQVs in ^{3}He-*A* remained elusive in experiments [6–10], as the spin-orbit interaction makes them unstable [11,12]. In the meantime, observations of half-quantum vortices and fluxes have been reported on the grain boundaries of *d*-wave cuprate superconductors [13], in chiral superconductor rings [14], and in Bose condensates [15,16]. In Bose systems, however, vortex-core-bound fermionic states do not exist, while in superconductors, only half-quantum fluxes not associated with a core (in Josephson vortices or rings) have so far been studied. Here we report the discovery of HQVs in the recently found polar phase of superfluid ^{3}He [17,18].

It is established that ^{3}He becomes superfluid by Cooper pairing in a state with spin 1 and orbital momentum 1, which is described by a 3×3 order-parameter matrix $A_{\mu j}$, where indices μ and j represent the spin and orbital degrees of freedom. The polar phase appears below the critical temperature $T_c \sim 10^{-3}$ K when liquid ^{3}He is confined in nafen [18], a commercially produced solid nanomaterial consisting of long strands aligned in the same direction $\hat{\mathbf{z}}$ [Fig. 1(a)]. In the polar phase, the order parameter has the form

$$A_{\mu j} = \Delta e^{i\phi} \hat{d}_\mu \hat{m}_j. \tag{1}$$

Here, Δ is the maximum gap in the quasiparticle energy spectrum, ϕ is the superfluid phase, $\hat{\mathbf{d}}$ is a unit vector of spin anisotropy, and $\hat{\mathbf{m}}$ is that of orbital anisotropy. Magnetic field $H > 3$ mT fixes $\hat{\mathbf{d}} = \hat{\mathbf{i}} \cos\alpha(\mathbf{r}) + \hat{\mathbf{j}} \sin\alpha(\mathbf{r})$, where $\hat{\mathbf{i}}$ and $\hat{\mathbf{j}}$ are mutually orthogonal unit vectors in the plane normal to $\mathbf{H}$. In the nafen, $\hat{\mathbf{m}}$ is pinned parallel to the strands, $\hat{\mathbf{m}} \| \hat{\mathbf{z}}$. The spin-orbit interaction $F_{\mathrm{SO}} \propto (\hat{\mathbf{d}} \cdot \hat{\mathbf{m}})^2$ then affects orientation of $\hat{\mathbf{d}}$ in such a way that the distribution of α is governed by the sine-Gordon equation (see the Supplemental Material [19] for details)

$$\nabla^2 \alpha = (\sin^2\mu / 2\xi_D^2) \sin 2\alpha, \tag{2}$$

where $\xi_D \sim 10$ μm is the dipole length, and μ is the angle of the magnetic field with respect to $\hat{\mathbf{z}}$ [Fig. 1(a)].

A quantized vortex is a linear topological defect in the order-parameter field which traps nonzero winding $\phi \to \phi + 2\pi\nu$ of the order-parameter phase ϕ on a path around the vortex core. Winding of the $\hat{\mathbf{d}}$ orientation given by the angle α is also possible. Thus, three different types of vortices may exist [Fig. 1(b)]: single-quantum vortices (SQVs), spin-current vortices (SCVs), and HQVs. SQVs are usual phase vortices with $\nu = 1$ associated with one quantum $\kappa = h/2m_3$ of mass circulation with velocity $\mathbf{v}_s = (\hbar/2m_3)\nabla\phi$ (m_3 is ^{3}He atom mass). In a SCV, $\alpha \to \alpha + 2\pi$ on a path around the core. It carries quantized circulation of spin current created by reorientation of the $\hat{\mathbf{d}}$ field. For a HQV, $\nu = 1/2$, and it carries only half a quantum $\kappa/2$ of mass circulation. The apparent phase jump by π is compensated by the change $\alpha \to \alpha + \pi$, which makes the order parameter single valued.

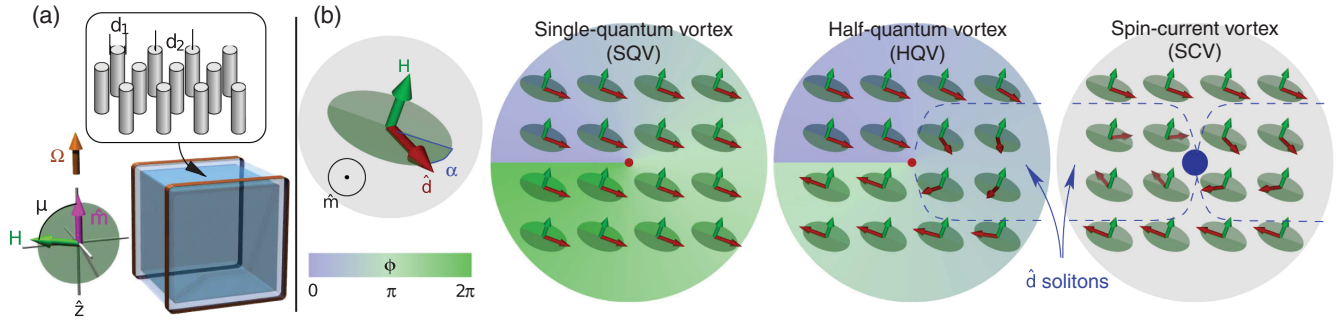

FIG. 1. (a) Sketch of the sample: Cubic container made from epoxy (light blue) is filled with the nafen (blue cube). The nafen strands are oriented along the vertical $\hat{\mathbf{z}}$ direction, their diameter is $d_1 \approx 9$ nm, and their average separation $d_2 \approx 35$ nm. The space between strands is filled with liquid ^{3}He. The sample is surrounded by nuclear magnetic resonance (NMR) coils made of copper wire (brown rectangles). The magnetic field $\mathbf{H}$ is applied transverse to the NMR coil axis at an arbitrary angle μ from the direction of the orbital anisotropy vector $\hat{\mathbf{m}}$, which is pinned along the nafen strands. The sample can be rotated around the vertical axis with the angular velocity Ω up to 3 rad/s. (b) Vortex types in the polar phase: The order-parameter phase ϕ is shown by the background colour. The spin vector $\hat{\mathbf{d}}$ is locked to the plane (green disks) perpendicular to the magnetic field $\mathbf{H}$. Within this plane, $\hat{\mathbf{d}}$ rotates by π around the HQV core and by 2π around the SCV core. In a tilted magnetic field ($\mu > 0$), this winding is concentrated in one $\hat{\mathbf{d}}$ soliton terminating at the HQV core or in two solitons terminating at the SCV core. The approximate soliton extents are illustrated by dashed lines. The nafen strands, the $\hat{\mathbf{m}}$ field, and the vortex lines are orthogonal to the plane of the picture. The SQV and HQV have hard cores (red disks) of the size of coherence length ~40 nm, while the SCV has only a soft core (blue disk) of much larger size ~10 μm.

Reorientation of $\hat{\mathbf{d}}$ outside of SCV and HQV cores is governed by well-known solitonic solutions of Eq. (2). The SCV becomes a termination line of two and HQV of one π soliton in the $\hat{\mathbf{d}}$ field. The soliton connects a HQV to another HQV with opposite $\hat{\mathbf{d}}$ winding (Supplemental Material [19], Fig. S1), to a SCV, or terminates at the sample boundary. The soliton width is $\sim\xi_D/\sin\mu$. In the absence of magnetic field or when the field is oriented along the nafen strands ($\mu = 0$), the spin-orbit energy $F_{\rm SO}$ is invariantly at the minimum for any $\hat{\mathbf{d}} \perp \hat{\mathbf{m}}$, and solitons are not created.

In our experiments, we use continuous-wave nuclear magnetic resonance (NMR). In the superfluid state, the spin-orbit coupling provides a torque acting on the precessing magnetization, which leads to a shift of the precession frequency from the Larmor value $\omega_L = |\gamma|H$, where $\gamma = -2.04 \times 10^8$ s^{-1} T^{-1} is the gyromagnetic ratio of ^{3}He. The sample regions where spin-orbit energy is at a minimum form the main peak in the NMR spectrum at the frequency $\omega_{\rm main}$ with the shift [46]

$$\Delta\omega_{\rm main} = \omega_{\rm main} - \omega_L = \frac{\Omega_P^2}{2\omega_L}\cos^2\mu. \qquad (3)$$

Here, Ω_P is the pressure- and temperature-dependent Leggett frequency in the polar phase, which characterizes the spin-orbit torque.

Within soft cores of topological objects, such as the $\hat{\mathbf{d}}$ solitons, the spin-orbit energy is not at minimum, which provides a trapping potential for standing spin waves. Excitation of these waves leads to a satellite peak in the NMR spectrum at the frequency $\omega_{\rm sat}$ with the shift

$$\Delta\omega_{\rm sat} = \omega_{\rm sat} - \omega_L = \frac{\Omega_P^2}{2\omega_L}(\cos^2\mu - \lambda\sin^2\mu). \qquad (4)$$

Here, $\lambda(\mu)$ is specific to the type of the topological object. For an infinite planar $\hat{\mathbf{d}}$ soliton, one has $\lambda = 1$, corresponding to the zero mode on the soliton [47]. In this case, one finds $\Delta\omega_{\rm sat}(\mu = \pi/2) = -\Delta\omega_{\rm main}(\mu = 0)$. For a $\hat{\mathbf{d}}$ soliton separating two HQVs, the signal is modified due to finite-size effects and also due to the Aharonov-Bohm effect for spin waves scattered on HQV cores (see the Supplemental Material [19]). In this respect, the HQV can be seen as an analogue of the Alice string in particle physics [48]. A particle that moves around an Alice string flips its charge [49], while a quasiparticle going around a HQV flips its spin quantum number. As a result, we expect $\lambda < 1$. The spin polarization of the HQV core predicted in Ref. [50] does not affect the signal, since for two HQVs bound by the soliton, the winding of $\hat{\mathbf{d}}$ (and, thus, spin polarization) is in the opposite directions.

In a sample rotating with angular velocity Ω, the lowest-energy state is achieved when superfluid mimics solid-body rotation with an array of rectilinear vortex lines oriented along the rotation direction, with density $n_v = 2\Omega/(\nu\kappa)$. In the polar phase, the spin-orbit interaction favors HQVs [51], and they are energetically preferable below T_c in the axial field (see the Supplemental Material [19]). However, when solitons are formed between HQV pairs in the tilted magnetic field, excess of the spin-orbit interaction energy within solitons makes SQVs preferable. Presumably, SCVs can be created during cooldown when strong time-dependent magnetic field is applied to generate a random distribution of vector $\hat{\mathbf{d}}$ [52]. Such experiments are beyond the scope of this work.

We approach the lowest-energy state by slowly cooling the sample in rotation from above T_c to the polar phase. The axis of rotation is parallel to the nafen strands [see

Fig. 1(a)]. The results presented in this work were obtained using 94% open nafen (density 243 mg/cm^3), at 7.1 bar pressure and magnetic field 12 mT. The corresponding NMR frequency is $\omega_L/2\pi = 374$ kHz. The temperature is measured from the NMR spectrum of the bulk B phase, using the known B-phase Leggett frequency [53,54]. As a secondary thermometer, we use a quartz tuning fork [55,56] located in bulk ^{3}He. Details of the experimental setup and methods are in the Supplemental Material [19].

In the experiment, when the magnetic field is oriented transverse to the nafen strands during cooldown, we observe only the bulk NMR line of the polar phase, which is consistent with the creation of SQVs. SQVs do not produce a potential well for spin waves and, thus, yield no satellite. When we apply no magnetic field or, alternatively, orient the field along the nafen strands during cooldown and then turn the field to the transverse direction below T_c, a satellite in the NMR spectrum is observed, Fig. 2(a). We interpret this satellite as produced by $\hat{\mathbf{d}}$ solitons connecting pairs of HQVs based on the following arguments.

First, the frequency of the satellite line conforms to expectations for a $\hat{\mathbf{d}}$ soliton. In Fig. 2, the frequency shift $-\Delta\omega_{\rm sat}(\mu = \pi/2)$ is compared to $\Delta\omega_{\rm main}(\mu = 0)$ as a function of temperature. They are seen to closely match each other, and we find $\lambda(\mu = \pi/2) = 0.93 \pm 0.07$. The deviation from ideal soliton value $\lambda = 1$ is expected to increase with decreasing field angle μ due to growing soliton width. This is qualitatively seen in Fig. 3.

In the analysis, we assume that the distance between vortex pairs defining the soliton length is independent of the angle μ, i.e., that the tension of the soliton is not able to overcome the pinning of HQV hard cores of the size of coherence length $\xi \sim 40$ nm on the nafen strands of $\sim$10 nm diameter. The strong pinning is confirmed by the observation that after stopping the rotation, the satellite in the NMR spectrum remains unchanged for days, while the Magnus force pulling vortices towards the sample boundary for annihilation exceeds the soliton tension by a factor of 10^3.

The second observation in support of HQV is the dependence of the relative satellite peak intensity $I_{\rm sat}$ on the angular velocity Ω of rotation, which is applied during the cooldown. The measured satellite intensity at $\mu = \pi/2$ is plotted in Fig. 4(a). For solitons of the ξ_D width between pairs of vortices, the expected signal is $I_{\rm sat} = (n_v/2)g_s L\xi_D$

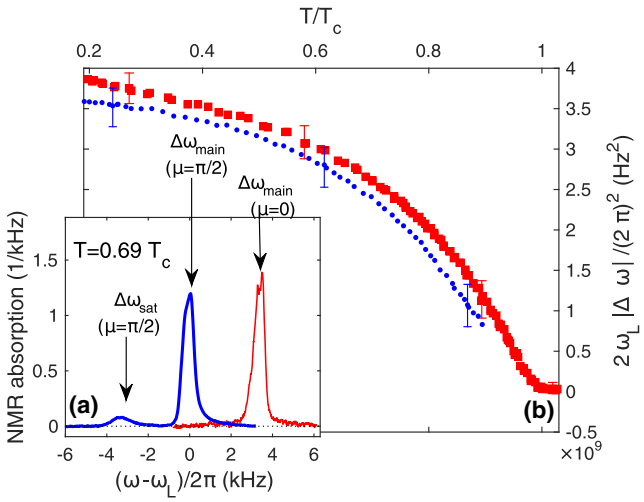

FIG. 2. NMR spectra in the polar phase with HQVs. (a) Normalized spectra measured in transverse field $\mu = \pi/2$ (blue thick line) show the HQV satellite at the negative frequency shift $\Delta\omega_{\rm sat}$ and the main line at zero frequency shift. In the axial field $\mu = 0$ (red thin line), only the main line at positive shift $\Delta\omega_{\rm main}$ is seen. This spectrum is not sensitive to presence of vortices. (b) Temperature dependences of the satellite position in the transverse field $|\Delta\omega_{\rm sat}(\mu = \pi/2)|$ (blue circles) and the main line position in the axial field $\Delta\omega_{\rm main}(\mu = 0)$ (red squares) closely match as expected for HQVs. The example error bars show full width at half maximum of non-Lorentzian main line as an estimate of possible systematic error.

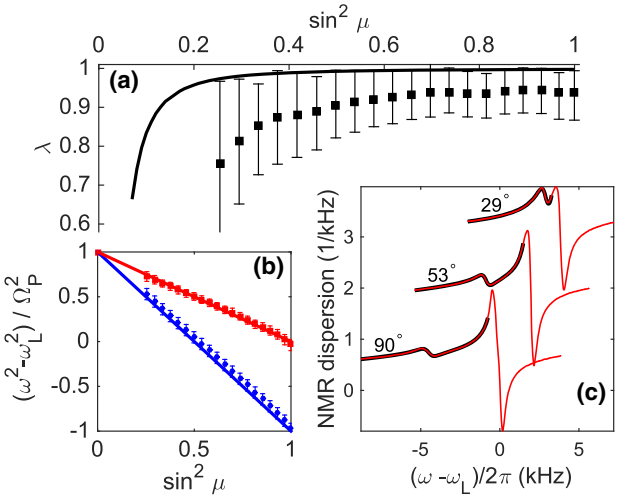

FIG. 3. Frequency shift of the HQV satellite in the NMR spectrum. (a) Measured values of the dimensionless frequency shift λ as a function of the field tilt angle μ (symbols) and numerical calculations for the uniform polar phase (solid line) using theoretical value of $\xi_D = 17$ μm [19]. Leggett frequency Ω_P is determined from a separate measurement at $\mu = 0$. As expected, the deviation from the infinitely long $\hat{\mathbf{d}}$ soliton value $\lambda = 1$ increases towards small μ. The disagreement between the experiment and calculations probably originates from disorder in the nafen strand orientation [57], which leads to fluctuations of spin-orbit interaction energy within the solitons. (b) Values of λ are found from positions of the HQV satellite $\Delta\omega_{\rm sat}$ (blue circles) and of the main line $\Delta\omega_{\rm main}$ (red squares). The red and blue solid lines show results of Eqs. (3) and (4), respectively, for $\lambda = 1$. (c) Main line and satellite line positions are determined using Lorentzian fits (thick black line) of the dispersion signal (red line). For clarity, the lines have been shifted vertically. Values of μ are marked above the lines. Similar fits are used in extracting the satellite line intensity in Fig. 4. In panels (a) and (b), the bars show full width at half maximum of the spectral lines.

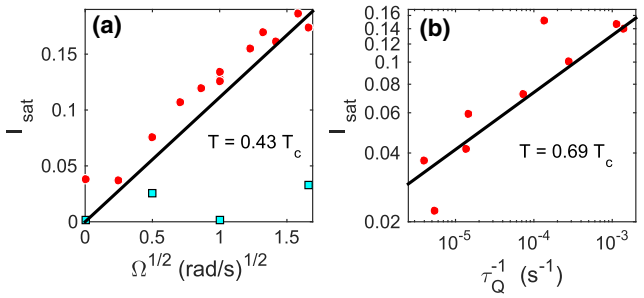

FIG. 4. Intensity $I_{\rm sat}$ of the HQV satellite in the NMR spectrum. (a) After cooldown in zero field (red circles), $I_{\rm sat}$ follows expected dependence for HQVs $I_{\rm sat} \propto \Omega^{1/2}$. The solid line is the theoretical prediction for the equilibrium array of HQVs ignoring Kibble-Zurek vortices and with no fitted parameters. For cooldowns in the transverse field (cyan squares), formation of HQVs is suppressed. Residual intensity is attributed to the possible formation of the soliton sheets terminating at the sample walls. The cooldown rate here is $\tau_Q^{-1} = 5 \times 10^{-6}$ s^{-1}. (b) For cooldowns at $\Omega = 0$ rad/s, the satellite intensity (symbols) follows dependence $I_{\rm sat} \propto \tau_Q^{-1/4}$ (solid line) expected for vortices created by the Kibble-Zurek mechanism, where the initial vortex density agrees with earlier measurements in ^{3}He-B [58]. In all cases, spectra are measured at $\mu = \pi/2$, and $I_{\rm sat}$ is determined as the area of the satellite normalized to the total area of the spectrum.

[9]. Here, $L = bn_v^{-1/2}$ is the average soliton length, where $g_s \sim 1$ is a numerical factor, which depends on the distribution of the trapped spin wave within the soliton. Numerical factor $b \sim 1$ depends on the vortex lattice. For very low vortex density and long solitons $L \to \infty$, one has $g_s \to 2$. As a result, one expects $I_{\rm sat} \propto \Omega^{1/2}$, as indeed seen in Fig. 4(a). Comparison of the measurements with the theoretical prediction for $I_{\rm sat}$ [19] shows good quantitative agreement, considering the absence of fitting parameters and simplicity of the model, which assumes uniform polar phase and uniform distribution of HQVs.

A remarkable feature seen in Fig. 4(a) is that the satellite appears in the zero-field cooldowns in the absence of rotation as well. We attribute this phenomenon to the Kibble-Zurek mechanism (KZ) of vortex (defect) formation [59,60] during the crossing of the second order phase transition to the polar phase. The KZ mechanism is expected to create various order-parameter defects including vortices of all possible types. In the earlier observations of vortex creation by the KZ mechanism in ^{3}He-B, initially formed vortices rapidly decayed [61–64]. In our case, the initially formed HQVs freeze due to the strong pinning. The scale for the intervortex distance is set by the KZ length $l_{\rm KZ} = \xi_0(\tau_Q/\tau_0)^{1/4}$. Here, $\tau_Q^{-1} = -[d(T/T_c)/dt]|_{T=T_c}$ is the cooldown rate at T_c, $\xi_0 = \xi(T = 0)$ and the order-parameter relaxation time $\tau_0 \sim 1$ ns. For HQVs, the intervortex distance sets the length of the interconnecting solitons and, thus, the amplitude of the satellite signal. The resulting dependence $I_{\rm sat} \propto l_{\rm KZ} \propto \tau_Q^{-1/4}$ is indeed observed in the experiment, Fig. 4(b). The magnitude of the signal corresponds to the averaged soliton length of $1.4l_{\rm KZ}$, as has been estimated as the initial intervortex distance also in the B phase of ^{3}He [58,64]. The shift of experimental data in Fig. 4(a) above the theoretical expectation indicates that the KZ mechanism is important also in cooldowns with applied rotation. A detailed analysis of the creation of various defects by the KZ mechanism in the presence of bias (rotation) and pinning remains a task for the future.

In conclusion, we cool ^{3}He within a nematically ordered aerogel-like material called nafen down to the superfluid polar phase in rotation up to 2.75 rad/s. When the cooldown proceeds without magnetic field or with the field oriented parallel to the nafen strands and rotation axis, and afterwards the field is switched on in the transverse direction, we observe a satellite peak in the continuous-wave NMR spectrum. Dependence of the satellite intensity and frequency on the rotation velocity, temperature, and field orientation identifies it as a signal from solitons between pairs of half-quantum vortices. Additionally, the frequency of the satellite reflects the Aharonov-Bohm effect for the spin waves scattered by the HQV core, which is the analogue of the transfer of the Cheshire charge in Alice electrodynamics [48]. The hard-core HQVs are strongly pinned by the nafen strands, which allows us to observe vortices created when passing through the transition temperature owing to the Kibble-Zurek mechanism even without rotation. If cooldown proceeds with the field applied in the transverse direction favoring stabilization of single-quantum vortices, no satellite is observed, as expected.

In less dense nafen (98% open, 90 mg/cm^3), the polar phase acquires axial distortion at low temperatures; i.e., it is transformed into the polar-distorted A phase [18]. The HQVs there contain unpaired Majorana modes in their cores similar to those discussed in HQVs in $p_x + ip_y$ superconductors or in "Kitaev chains" [3–5]. Since the HQVs are trapped by the nafen columnar defects, the gap separating the Majorana mode from the other Caroli–de Gennes–Matricon excitations localized in the vortex core increases from the usual minigap value $\sim\Delta^2/E_F \sim 10^{-3}\Delta$ (here, E_F is the Fermi energy) in an unpinned vortex to a significant fraction of the gap amplitude Δ for a vortex trapped on a defect [65,66]. Our preliminary results of HQV measurements in the 98% open nafen show that HQVs survive the transition from the polar phase to the polar-distorted A phase. This opens a pathway for probing the core-bound unpaired Majorana modes in the experimentally accessible temperature range in the polar-distorted A phase and also in the new topological phases obtained using properly engineered nanostructured confinement [19], while the Kibble-Zurek mechanism makes the HQVs accessible with less specialized, stationary equipment.

This work has been supported by the Academy of Finland (Projects No. 284594 and No. 298451) and

Russian Foundation for Basic Research Grant No. 16-02-00349. We used facilities of the Low Temperature Laboratory infrastructure of Aalto University. S. A. acknowledges financial support from the Finnish Cultural Foundation. We thank I. M. Grodnensky for providing the nafen samples.

*samuli.autti@aalto.fi

[1] G. E. Volovik, *The Universe in a Helium Droplet* (Oxford University Press, New York, 2003).
[2] T. Mizushima, Y. Tsutsumi, T. Kawakami, M. Sato, M. Ichioka, and K. Machida, J. Phys. Soc. Jpn. **85**, 022001 (2016).
[3] G. E. Volovik, JETP Lett. **70**, 609 (1999).
[4] N. Read and D. Green, Phys. Rev. B **61**, 10267 (2000).
[5] D. A. Ivanov, Phys. Rev. Lett. **86**, 268 (2001).
[6] G. E. Volovik and V. P. Mineev, JETP Lett. **24**, 561 (1976).
[7] M. C. Cross and W. F. Brinkman, J. Low Temp. Phys. **27**, 683 (1977).
[8] M. M. Salomaa and G. E. Volovik, Phys. Rev. Lett. **55**, 1184 (1985).
[9] C.-R. Hu and K. Maki, Phys. Rev. B **36**, 6871 (1987).
[10] T. Kawakami, Y. Tsutsumi, and K. Machida, Phys. Rev. B **79**, 092506 (2009).
[11] P. J. Hakonen, K. K. Nummila, J. T. Simola, L. Skrbek, and G. Mamniashvili, Phys. Rev. Lett. **58**, 678 (1987).
[12] M. Yamashita, K. Izumina, A. Matsubara, Y. Sasaki, O. Ishikawa, T. Takagi, M. Kubota, and T. Mizusaki, Phys. Rev. Lett. **101**, 025302 (2008).
[13] J. R. Kirtley, C. C. Tsuei, M. Rupp, J. Z. Sun, L. S. Yu-Jahnes, A. Gupta, M. B. Ketchen, K. A. Moler, and M. Bhushan, Phys. Rev. Lett. **76**, 1336 (1996).
[14] J. Jang, D. G. Ferguson, V. Vakaryuk, R. Budakian, S. B. Chung, P. M. Goldbart, and Y. Maeno, Science **331**, 186 (2011).
[15] K. G. Lagoudakis, T. Ostatnický, A. V. Kavokin, Y. G. Rubo, R. André, and B. Deveaud-Plédran, Science **326**, 974 (2009).
[16] S. W. Seo, S. Kang, W. J. Kwon, and Y.-i. Shin, Phys. Rev. Lett. **115**, 015301 (2015).
[17] K. Aoyama and R. Ikeda, Phys. Rev. B **73**, 060504 (2006).
[18] V. V. Dmitriev, A. A. Senin, A. A. Soldatov, and A. N. Yudin, Phys. Rev. Lett. **115**, 165304 (2015).
[19] See the Supplemental Material at http://link.aps.org/supplemental/10.1103/PhysRevLett.117.255301, which includes Refs. [20–45], for description of the experimental setup and methods, comparison of vortex energies in the polar phase, calculation of the NMR properties of the polar phase, and an overview of the topological phases of superfluid ^{3}He.
[20] P. J. Heikkinen, S. Autti, V. B. Eltsov, R. P. Haley, and V. V. Zavjalov, J. Low Temp. Phys. **175**, 681 (2014).
[21] I. Todoshchenko, J. P. Kaikkonen, R. Blaauwgeers, P. J. Hakonen, and A. Savin, Rev. Sci. Instrum. **85**, 085106 (2014).
[22] Y. A. Ono, J. Hara, and K. Nagai, J. Low Temp. Phys. **48**, 167 (1982).
[23] M. M. Salomaa and G. E. Volovik, Rev. Mod. Phys. **59**, 533 (1987).
[24] Y. M. Bunkov and O. D. Timofeevskaya, Phys. Rev. Lett. **80**, 4927 (1998).
[25] E. V. Thuneberg, J. Low Temp. Phys. **122**, 657 (2001).
[26] E. V. Thuneberg, arXiv:cond-mat/9802044.
[27] V. V. Zavjalov, arXiv:1601.04190.
[28] T. D. C. Bevan, A. J. Manninen, J. B. Cook, J. R. Hook, H. E. Hall, T. Vachaspati, and G. E. Volovik, Nature (London) **386**, 689 (1997).
[29] N. B. Kopnin and M. M. Salomaa, Phys. Rev. B **44**, 9667 (1991).
[30] S.-M. Huang, S.-Y. Xu, I. Belopolski, C.-C. Lee, G. Chang, B. Wang, N. Alidoust, G. Bian, M. Neupane, C. Zhang, S. Jia, A. Bansil, H. Lin, and M. Z. Hasan, Nat. Commun. **6**, 7373 (2015).
[31] L. Lu, Z. Wang, D. Ye, L. Ran, L. Fu, J. D. Joannopoulos, and M. Soljačić, Science **349**, 622 (2015).
[32] T. Mizushima, Y. Tsutsumi, M. Sato, and K. Machida, J. Phys. Condens. Matter **27**, 113203 (2015).
[33] S. Murakawa, Y. Wada, Y. Tamura, M. Wasai, M. Saitoh, Y. Aoki, R. Nomura, Y. Okuda, Y. Nagato, M. Yamamoto, S. Higashitani, and K. Nagai, J. Phys. Soc. Jpn. **80**, 013602 (2011).
[34] Y. M. Bunkov, J. Low Temp. Phys. **175**, 385 (2014).
[35] A. P. Schnyder and S. Ryu, Phys. Rev. B **84**, 060504 (2011).
[36] A. P. Schnyder and P. M. R. Brydon, J. Phys. Condens. Matter **27**, 243201 (2015).
[37] R. Yu, H. Weng, Z. Fang, X. Dai, and X. Hu, Phys. Rev. Lett. **115**, 036807 (2015).
[38] Y. Kim, B. J. Wieder, C. L. Kane, and A. M. Rappe, Phys. Rev. Lett. **115**, 036806 (2015).
[39] T. T. Heikkilä and G. E. Volovik, New J. Phys. **17**, 093019 (2015).
[40] G. E. Volovik, arXiv:1509.05006.
[41] Y. Makhlin, M. Silaev, and G. E. Volovik, Phys. Rev. B **89**, 174502 (2014).
[42] A. B. Vorontsov and J. A. Sauls, Phys. Rev. Lett. **98**, 045301 (2007).
[43] G. E. Volovik and V. M. Yakovenko, J. Phys. Condens. Matter **1**, 5263 (1989).
[44] G. E. Volovik and L. P. Gorkov, Sov. Phys. JETP **61**, 843 (1985).
[45] M. Creutz, J. High Energy Phys. 04 (2008) 017.
[46] V. P. Mineev, J. Low Temp. Phys. **184**, 1007 (2016).
[47] D. Vollhardt and P. Wölfle, *The Superfluid Phases of Helium 3* (Dover Publications, New York, 2013).
[48] C. Wu, J. Hu, and S.-C. Zhang, Int. J. Mod. Phys. B **24**, 311 (2010).
[49] A. S. Schwarz, Nucl. Phys. **B208**, 141 (1982).
[50] V. Vakaryuk and A. J. Leggett, Phys. Rev. Lett. **103**, 057003 (2009).
[51] V. P. Mineev, J. Low Temp. Phys. **177**, 48 (2014).
[52] V. V. Dmitriev, D. A. Krasnikhin, N. Mulders, A. A. Senin, G. E. Volovik, and A. N. Yudin, JETP Lett. **91**, 599 (2010).
[53] E. V. Thuneberg, J. Low Temp. Phys. **122**, 657 (2001).
[54] P. J. Hakonen, M. Krusius, M. M. Salomaa, R. H. Salmelin, J. T. Simola, A. D. Gongadze, G. E. Vanchnadze, and G. A. Kharadze, J. Low Temp. Phys. **76**, 225 (1989).
[55] R. Blaauwgeers, M. Blažková, M. Človečko, V. B. Eltsov, R. de Graaf, J. Hosio, M. Krusius, D. Schmoranzer,

W. Schoepe, L. Skrbek, P. Skyba, R. E. Solntsev, and D. E. Zmeev, J. Low Temp. Phys. **146**, 537 (2007).
[56] M. Blažková, M. Človečko, V. B. Eltsov, E. Gažo, R. de Graaf, J. J. Hosio, M. Krusius, D. Schmoranzer, W. Schoepe, L. Skrbek, P. Skyba, R. E. Solntsev, and W. F. Vinen, J. Low Temp. Phys. **150**, 525 (2008).
[57] V. E. Asadchikov, R. S. Askhadullin, V. V. Volkov, V. V. Dmitriev, N. K. Kitaeva, P. N. Martynov, A. A. Osipov, A. A. Senin, A. A. Soldatov, D. I. Chekrygina, and A. N. Yudin, JETP Lett. **101**, 556 (2015).
[58] C. Bäuerle, Y. M. Bunkov, S. N. Fisher, H. Godfrin, and G. R. Pickett, J. Low Temp. Phys. **110**, 13 (1998).
[59] T. W. B. Kibble, J. Phys. A **9**, 1387 (1976).
[60] W. H. Zurek, Nature (London) **317**, 505 (1985).
[61] V. M. H. Ruutu, V. B. Eltsov, A. J. Gill, W. B. Kibble, M. Krusius, Y. G. Makhlin, B. Plaçais, G. E. Volovik, and W. Xu, Nature (London) **382**, 334 (1996).
[62] C. Bäuerle, Y. M. Bunkov, S. N. Fisher, H. Godfrin, and G. R. Pickett, Nature (London) **382**, 332 (1996).
[63] Y. M. Bunkov, A. I. Golov, V. S. L'vov, A. Pomyalov, and I. Procaccia, Phys. Rev. B **90**, 024508 (2014).
[64] V. B. Eltsov, M. Krusius, and G. E. Volovik, *Progress in Low Temperature Physics* (Elsevier, New York, 2005), Vol. XV, pp. 1–137.
[65] A. S. Mel'nikov, A. V. Samokhvalov, and M. N. Zubarev, Phys. Rev. B **79**, 134529 (2009).
[66] B. Rosenstein, I. Shapiro, and B. Y. Shapiro, J. Phys. Condens. Matter **25**, 075701 (2013).